Materials Physics and Mechanics 47 (2021) 219-236 Received: June 24, 2020

MODIFIED DUGDALE MODEL FOR MULTIPLE CIRCULAR ARC-CRACKS WITH UNIFIED PLASTIC ZONES: A COMPLEX VARIABLE APPROACH

Naved Akhtar*, S. Hasan

Department of Mathematics, Jamia Millia Islamia, New Delhi-110 025, India.

*e-mail: naved.a86@gmail.com

Abstract. A crack arrest model is presented in this paper for multiple circular arc-cracks with coalesced yield zones. The geometry of cracks discussed in the article assumes as a prelude to the case of two equal circular arc-cracks. Further, the influence of variable stress distribution on the rims of the cracks is studied. Analytical expressions for stress intensity factors and applied load ratios are obtained using the complex variable method. Numerical results are obtained for applied load ratio, yield zone length, and reported graphically.
Keywords: circular-arc cracks, Dugdale strip-yield model, yield zone length, stress intensity factor

1. Introduction

Due to considerable mathematical difficulties, the journey of determining the precise residual strength of engineering materials is always a hard nut to crack. Particularly, when the material is damaged due to the development/ presence of multiple cracks or crack-like defects. In the case of multiple cracks, two or more closely located small cracks when interacting with each other form a big crack, which may cause a severe problem to the integrity of the structure. Before the formation of a big crack, the yield zones developed at each internal tip of the cracks get coalesced due to an increase in applied stress at the infinite boundary of the plate.

The residual strength of the structure containing cracks is inversely proportional to the crack size. Therefore, it is imperative to evaluate the residual strength of the structure as a function of crack size. In this connection, Dugdale [1] formulated the relationship between the residual strength of the structure and the crack size, which is now known as the Dugdale strip yield model. However, the model was used largely to study the size of the yield zone in the case of straight cracks. Moreover, the geometry of the crack also makes an impression on the residual strength of the structure. Therefore, large of work has been done in past to study the problem of multiple circular-arc cracks which includes the work of Smith [2], Chen [3], [4], Bhargava et al. [5], [6], Jagannadham [7], Zhang [8], etc. The problem of circular arc cracks may be considered as a generalization to the Dugdale model due to the complexity of the crack geometries.

Furthermore, the problem of circular-arc cracks, using different mathematical approaches, was discussed by several researchers e.g., Shiah [9] used a complex variable approach to solve a circular arc crack under partial loading conditions and Zhong et al. [10] used it to analyze the problem of a circular arc-crack in piezoelectric materials under antiplane shear and in-plane

http://dx.doi.org/10.18149/MPM.4722021_5

electric field. Gao et al. [11] used Green's function approach for the treatment of a circular arc-crack at the interface between a circular piezoelectric material and an infinite matrix. Semi inverse method used to solve the problem of arc crack by Shen et al. [12]. The boundary collocation method was applied by Cheung et al. [13] to calculate the stress intensity factor at the crack tip of a circular-arc crack in an infinite plate. Bhargava et al. [14] using the complex variable approach obtained the analytical expressions of the residual strength of an infinite isotropic plate containing a single circular arc crack. Gdoutos et al. [15] discussed the problem of two asymmetric circular arc cracks in an infinite isotropic plate and also the case of two equal and symmetrically positioned cracks. Bhargava et al. [16] addressed the issue of coalescence of yield zones between two adjacent circular-arc cracks. The theoretical and experimental study is carried for various arrangements of arc cracks by Pourseifi [17]. Stress intensity factors for circular-arc cracks in finite plates were calculated using finite element analysis by Shim et al. [18].

In the present study, an effort has been made to obtain a closed-form expression for the residual strength of a damaged plate in the presence of four circular-arc cracks with unified yield zones. Thomson's [19] and Muskhelishvili's [20] complex variable approach is used to obtain analytical expressions for stress intensity factor, yield zone ratio at each crack tip. The Crack-arrest model under general yielding condition was discussed recently [21] for similar cracks configuration.

2. Circular-arc-crack problem

A schematic diagram of the problem of four circular-arc cracks with coalesced yield zones is depicted in two Fig. 1 and Fig. 2. The cracks, $L_i(i = 1,2,3,4)$, occupy the intervals $[b_1 = Re^{-i\beta}$, $d_1 = Re^{-i\gamma}]$, $[c_1 = Re^{i\gamma}$, $a_1 = Re^{i\beta}]$, $[-b_1 = -Re^{-i\beta}$, $-d_1 = -Re^{-i\gamma}]$, and $[-c_1 = -Re^{i\gamma}$, $-a_1 = -Re^{i\beta}]$, respectively on the circumference of a circle $|z| = R$ in an infinite elastic perfectly-plastic plate occupy the entire complex-plane.

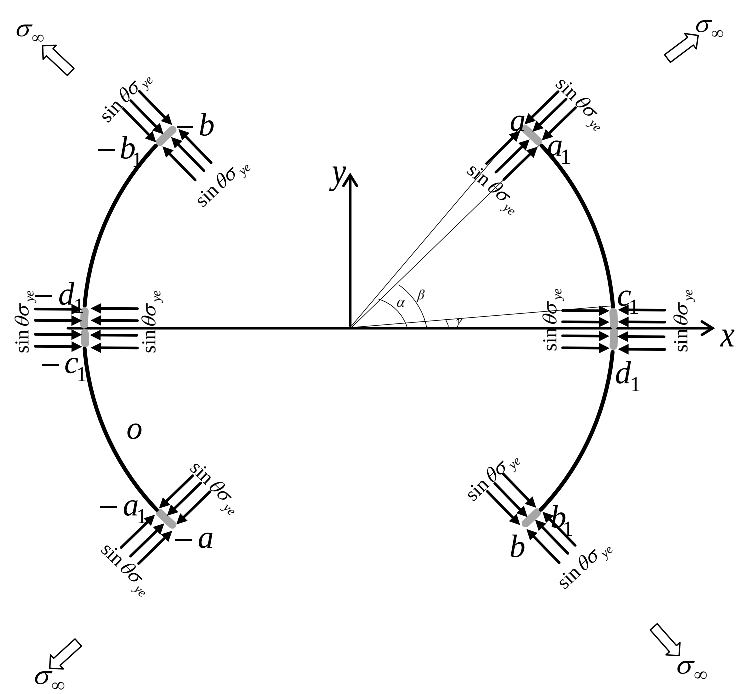

Fig. 1. Configuration of the problem when loading condition $\sin\theta\,\sigma_{ye}$

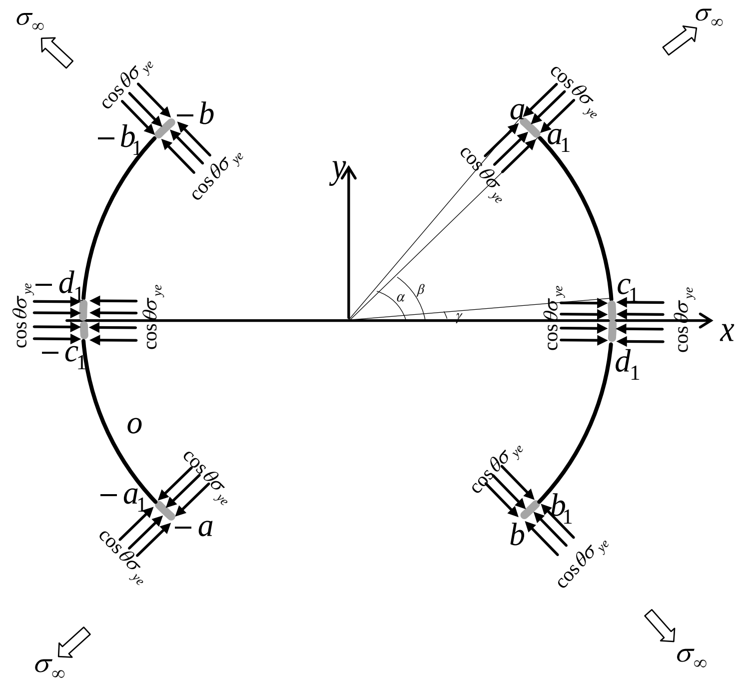

Fig. 2. Configuration of the problem when loading condition $\cos\theta\,\sigma_{ye}$

Rims of the cracks open in mode-I type deformation as the infinite boundary of the plate are subjected to stress distribution σ_∞. As a result, the formation of yield zones takes place at each crack tip. Stresses applied at the infinite boundary of the plate increases to such a limit that the yield zones developed at the inner crack tips d_1, c_1 and $-d_1$, $-c_1$ get coalesced.

The yield zones together with the coalesced yield zones are denoted by $\Gamma_j (j = 1,2,3,4,5,6)$ and occupy the intervals $(b = Re^{-i\alpha}, b_1 = Re^{-i\beta})$, $(d_1 = Re^{-i\gamma}, c_1 = Re^{i\gamma})$, $(a_1 = Re^{i\beta}, a = Re^{i\alpha})$, $(-b = -Re^{-i\alpha}, -b_1 = -Re^{-i\beta})$, $(-d_1 = -Re^{-i\gamma}, -c_1 = -Re^{i\gamma})$, $(-a_1 = -Re^{i\beta}, -a = -Re^{i\alpha})$, respectively on one and the same circle $|Z| = R$.

According to Gdoutos [22], materials may fail at stresses that are well below the yield stress of the material. Therefore, to study the behavior of yield zone length under the influence of variable yield stress distribution. Two different types of stress distributions have to be distinguished. First $\sigma_{rr} = \sin\theta\sigma_{ye}$ as shown in Fig. 1 and second $\sigma_{rr} = \cos\theta\sigma_{ye}$ presented in Fig. 2., where σ_{ye} is the yield stress of the material and $t = Re^{i\theta}$ is any point on the rims of the yield zones. Moreover, the article discussed two different cases of remotely applied stress. Firstly, when the infinite boundary is subjected to a uniform stress distribution as shown in Fig. 3 and second when remote stress reduces to tension p making an angle ξ with positive x −axis, shown in Fig. 4.

3. Solution of the circular-arc-crack problem

The solution of the problem discussed in section 2 for multiple interacting circular-arc cracks is obtained by dividing the problem into two different sub-problems, namely, opening case and closing case and denoted by subproblem-A and subproblem-B respectively. These subproblems are solved separately, and the solution of the main problem is then obtained by superposing the solutions of them.

Subproblem-A and its solution. The problem discussed in this section is related to the case of opening of circular-arc cracks due to remotely applied stresses at the infinite boundary of the plate. These cracks are assumed to be open in mode-I type deformation. Two different types of stress profiles were used to analyze the opening of the cracks theoretically. These cases of two different stress profiles, as shown in Fig. 3 and Fig. 4, are discussed here.

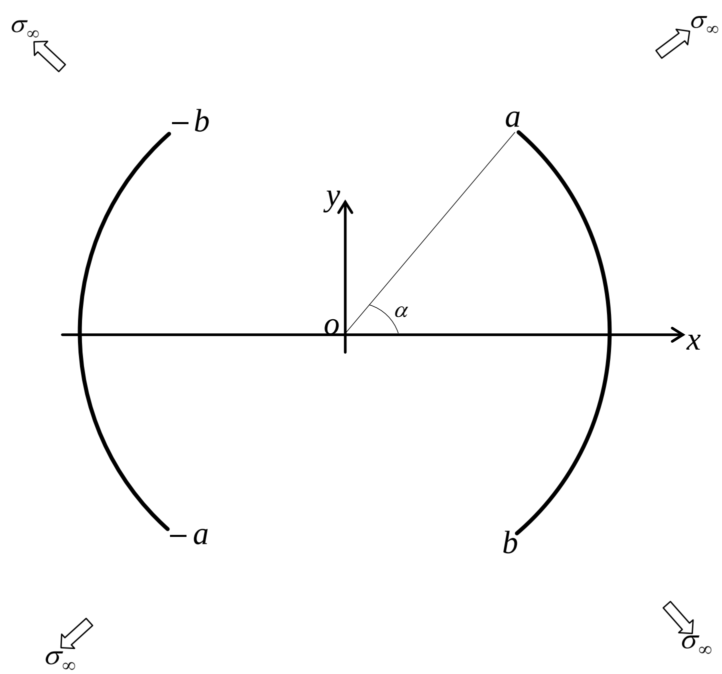

Fig. 3. Configuration of the Sub-problem A: uniform stress distribution σ_∞

Case-I: uniform tensile stress distribution. Consider the boundary of the plate is subjected to uniform remotely applied stress distribution, as shown in Fig. 3. Four circular arc cracks, weaken the plate, open in mode-I type deformation. In this case, the boundary conditions are:

1. Remote stresses are distributed equally in all directions ($\sigma_{rr}^{\pm} = \sigma_\infty$).
2. Rotation vanishes at the infinite boundary of the plate.
3. Body forces are absent.
4. Displacement components are single-valued throughout the plate.

Using the above boundary conditions and the mathematical formulation given in Appendix-A the complex potential function for the opening case of the problem is,

$$\Phi_A^m(z) = \frac{\sigma_\infty}{2(2-H^2)}\left\{1 - H^2 + \frac{z^2 + R^2(1-2H^2)}{X(z)}\right\}, \tag{1}$$

where $H^2 = E(k)/F(k)$ and $F(k)$, $E(k)$ are complete elliptical integral of first and second kind respectively as defined by Byrd [23], $k = \sin\alpha$. The superscript m indicates that the function refers to the stress profile shown in Fig. 3.

Stress intensity factor at the crack tip $a = Re^{i\alpha}$ for opening mode may be calculated by substituting $\Phi_A^m(z)$ from equation (1) into (41),

$$(K_A^m)_I = \frac{\sigma_\infty\sqrt{R\pi}}{2-H^2}\left(H^2\sqrt{\tan\alpha} - i(1-H^2)\sqrt{\cot\alpha}\right), \tag{2}$$

here subscript I refer to the mode-I (opening mode) type of deformation.

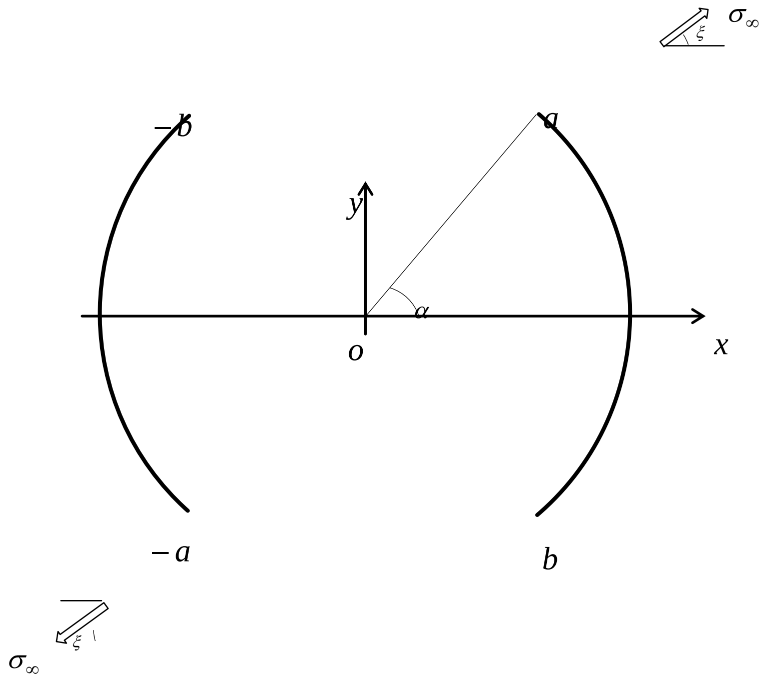

Fig. 4. Configuration of the Sub-problem A: stresses acting at an angle ξ to the ox-axis

Case-II: tensile stress distribution at a point. In this section, the case when applied remote stress reduces to a tension $\boldsymbol{p}$ acting in the direction, making an angle $\boldsymbol{\xi}$ with $\boldsymbol{ox}$-axis as depicted in Fig. 4 will be discussed. In view of that, the boundary conditions of the problem are as follows,

1. Remote stresses $\sigma_{rr}^{\pm} = \sigma_\infty$, $\sigma_{r\theta}^{\pm} = 0$ are applied in a direction making an angle ξ with ox-axis.
2. The rims of the cracks are stress-free.
3. Body forces are absent.
4. Displacement components are single-valued throughout the plate.

The complex potential function is then obtained under the boundary conditions and mathematical formulation given in Appendix-A yields the following

$$\Phi_A^n(z) = \frac{\sigma_\infty}{8}\left[\left(\frac{z^2 + R^2(1-2H^2)}{X(z)} - 1\right)Q_2 - \frac{2R^2 e^{2i\xi}}{z^2}\left(\frac{R^2}{X(z)} + 1\right)\right] \tag{3}$$

where

$$Q_2 = \frac{2 + \cos 2\xi \cos 2\alpha}{2 - H^2} - i\frac{\sin 2\xi \cos 2\alpha}{H^2},$$

superscript n refers to the stress profile shown in Fig. 4.

The state of stresses in the crack tip $z = Re^{i\alpha}$ may be obtained using equations (3) and (41) as

$$(K_A^n)_I = K_1 - iK_2 \tag{4}$$

where,

$$K_1=\frac{\sigma_\infty}{2}\sqrt{R\pi\tan\alpha}\left\{\frac{H^2}{2-H^2}+\cos 2\xi\left(2+\cos^2\alpha-\frac{2(1+\sin^2\alpha)}{2-H^2}\right)\right.$$
$$\left.+\sin 2\xi\cot\alpha\left(1+\sin^2\alpha-\frac{\cos^2\alpha}{H^2}\right)\right\},$$
$$K_2=\frac{\sigma_\infty}{2}\sqrt{R\pi\cot\alpha}\left\{\frac{1-H^2}{2-H^2}-\cos 2\xi\left(\cos^2\alpha-\frac{1+\sin^2\alpha}{2-H^2}\right)-\sin 2\xi\sin\alpha\cos\alpha\right\}.$$

Subproblem-B and its solution. The study of variable pressure arresting of arc cracks, in an infinite isotropic plate, is the main objective of subproblem-B. Presence of these cracks $\mathbf{L_i}(\mathbf{i}=\mathbf{1},\mathbf{2},\mathbf{3},\mathbf{4})$ with unified yield zones $(\mathbf{\Gamma_j},\mathbf{j}=\mathbf{1},\mathbf{2},\dots,\mathbf{6})$ influence the strength of the plate. Variable stress distribution applied over the rims of the developed yield zones seized the opening of cracks. Two different stress profiles of closing stresses are discussed in this section.

1. Yield stresses are distributed in the form of $\sigma_{rr}=\sin\theta\sigma_{ye}$, as shown in Fig. 5.
2. Yield stresses are distributed in the form of $\sigma_{rr}=\cos\theta\sigma_{ye}$, as shown in Fig. 6.

Case of $\boldsymbol{\sigma_{rr}=sin\theta\sigma_{ye}}$. The yield zones, developed at each crack tip of four circular arc cracks with unified yield zones, are subjected to a variable stress distribution $\boldsymbol{\sigma_{rr}=\sin\theta\sigma_{ye}}$ as shown in Fig. 5. To arrest the further opening of these cracks. Therefore, the boundary conditions for this case are as follows:

1. Rims of yield zones are subjected to $\sigma_{rr}=\sin\theta\sigma_{ye}$.
2. Boundary of the plate is stress-free.
3. Body forces are absent.
4. Displacement components are single-valued throughout the plate.

Using methodology is given in Appendix-A and above boundary conditions, the complex potential function for this case is

$$\Phi_{B_1}(z)=\frac{\sigma_{ye}}{2\pi iX(z)}\int_\Gamma\frac{X(t)\sin\theta}{t-z}dt+\frac{1}{2X(z)}\{C_0z^2+C_2\}+\frac{D_0}{2},\tag{5}$$

where C_0, C_2 and D_0 are the constants to be determined using the boundary conditions, and $X(z)=\sqrt{z^2-R^2e^{2i\alpha}}\sqrt{z^2-R^2e^{-2i\alpha}}$, $\left(\Gamma=\bigcup_{j=1}^{6}\Gamma_j\right)$, Γ_j denotes the yield zones.

Integral on the right-hand side of the equation (5) is solved by substituting $\sin\theta=\frac{t-\bar{t}}{2i}$ and $t\bar{t}=R^2$. Thus,

$$\int_\Gamma\frac{X(t)\sin\theta}{t-z}dt\tag{6}$$
$$=-\frac{1}{a}\left[S_1+\left(z^2-R^2(1+2\cos 2\alpha)\right)S_2+\left(z^4-R^2(z^2-R^2)(1+2\cos 2\alpha)\right)S_3\right.$$
$$\left.-(z^2-b^2)(z^2-R^2)S_4\right].$$

where,

$$S_1=\frac{a^4}{3}\left((k^2-1)S_3-2(k^2-2)\frac{S_2}{a^2}+k^2S_5\right),$$
$$S_2=a^2(E(\theta_1,k)-E(\theta_2,k)+E(k)-E(\theta_3,k)+E(\theta_4,k)),$$
$$S_3=F(\theta_1,k)-F(\theta_2,k)+F(k)-F(\theta_3,k)+F(\theta_4,k),$$
$$S_4=\Pi(\theta_1,\alpha^2,k)-\Pi(\theta_2,\alpha^2,k)+\Pi\left(\frac{\pi}{2},\alpha^2,k\right)-\Pi(\theta_3,\alpha^2,k)+\Pi(\theta_4,\alpha^2,k)),$$

$$S_5 = \sin\theta_1\cos\theta_1\sqrt{1-k^2\sin^2\theta_1} - \sin\theta_2\cos\theta_2\sqrt{1-k^2\sin^2\theta_2} - \sin\theta_3\cos\theta_3\sqrt{1-k^2\sin^2\theta_3} + \sin\theta_4\cos\theta_4\sqrt{1-k^2\sin^2\theta_4},$$

$$\theta_1 = \sqrt{\frac{e^{2i\alpha}-e^{2i\beta}}{e^{2i\alpha}-e^{-2i\alpha}}}, \theta_2 = \sqrt{\frac{e^{2i\alpha}-e^{-2i\beta}}{e^{2i\alpha}-e^{-2i\alpha}}}, \theta_3 = \sqrt{\frac{e^{2i\alpha}-e^{2i\gamma}}{e^{2i\alpha}-e^{-2i\alpha}}}, \theta_4 = \sqrt{\frac{e^{2i\alpha}-e^{-2i\gamma}}{e^{2i\alpha}-e^{-2i\alpha}}},$$

$$\alpha^2(z) = \frac{a^2-b^2}{a^2-z^2}, k^2 = 1-e^{-4i\alpha}.$$

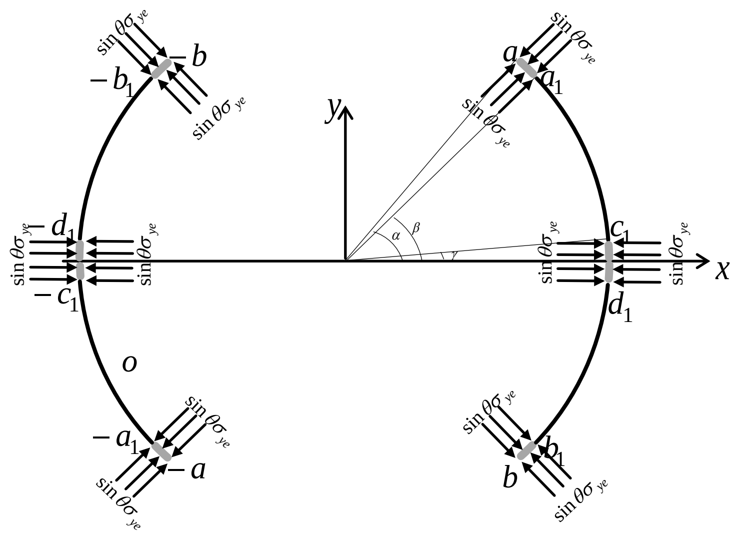

Fig. 5. Configuration of the closing case for $\sin\theta\sigma_{ye}$ loading

Constants given in equation (5) are obtained using the condition of single valuedness of displacement and loading conditions of the problem

$$C_0 = \frac{\sigma_{ye}}{i\alpha\pi(3-\cos2\alpha)}\left(\frac{S_1}{R^2} - 2\cos2\alpha S_2 + R^2\cos2\alpha S_3 - b^2(S_4-\overline{S_4}) + 2R^2\sin^2\alpha\overline{S_4} + 2G_1 - G_3 - G_4S_4 + G_2(S_4+\overline{S_4})\right) = \frac{\sigma_{ye}}{i\alpha\pi}C_{00}, \tag{7}$$

$$C_2 = \frac{R^2\sigma_{ye}}{i\alpha\pi}(G_3+G_4S_4) - C_0R^2\cos2\alpha = \frac{R^2\sigma_{ye}}{i\alpha\pi}C_{22}, \tag{8}$$

$$D_0 = \frac{\sigma_{ye}}{i\alpha\pi}(G_1+G_2S_4) - C_0, \tag{9}$$

$$G_1 = S_2 - 2R^2\cos^2\alpha S_3, \tag{10}$$

$$G_2 = 2R^2\sin^2\alpha + b^2, \tag{11}$$

$$G_3 = \frac{S_1}{R^2} - 2\cos^2\alpha S_2 + \frac{R^2}{4}(1+4\cos2\alpha-\cos4\alpha)S_3, \tag{12}$$

$$G_4 = \frac{R^2}{2}(3\sin^2 2\alpha - 4\sin^2\alpha(1+e^{-2i\alpha})). \tag{13}$$

Hence, substituting equations (6 – 13) into the equation (5), one gets the closed-form of the complex potential function for this case,

$$\Phi_{B_1}(z) = -\frac{\sigma_{ye}}{2ia\pi X(z)}[S_1 + (z^2 - R^2(1 + 2\cos 2\alpha))S_2 + (z^4 - R^2(z^2 - R^2)(1 + 2\cos 2\alpha))S_3 - (z^4 - z^2R^2 - b^2(z^2 - R^2))S_4] + \frac{C_0 z^2 + C_2}{2X(z)} + \frac{D_0}{2}. \quad (14)$$

The stress intensity factor is obtained by putting the value of $\Phi_{B_1}(z)$ from equation (14) into the equation (41) and can be written as,

$$K^I_{B_1} = \frac{\sigma_{ye}\sqrt{R}}{ae^{i\alpha}\sqrt{2\pi\sin 2\alpha}}\left[\frac{S_1}{R^2} - (1 + e^{-2i\alpha})S_2 + R^2e^{-2i\alpha}S_3 - R^2(e^{4i\alpha} - 1 - 2i\sin 2\alpha)S_4 - C_{00}e^{2i\alpha} - C_{22}\right]. \quad (15)$$

Case of $\boldsymbol{\sigma_{rr} = \cos\theta\sigma_{ye}}$. In this case, rims of the yield zone are subjected to stress distribution $\boldsymbol{\sigma_{rr} = \cos\theta\sigma_{ye}}$ and $\boldsymbol{\sigma_{r\theta}}$=0. Pictorial representation for this case is given in Fig. 6.

The complex potential functions for the case, when variable stress $\cos\theta\sigma_{ye}$ is distributed over the rims of yield zones, may be written as

$$\Phi_{B_2}(z) = \frac{\sigma_{ye}}{2\pi i X(z)}\int_\Gamma \frac{\cos\theta X(t)}{t - z}dt + \frac{1}{2X(z)}\{C_0z^2 + C_2\} + \frac{D_0}{2}, \quad (16)$$

where C_0, C_2 and D_0 are the constants and subscript B_2 refers to the case of compressing stress profile $\cos\theta\sigma_{ye}$.

Using well-known relation $2\cos\theta = t + \bar{t}$. The integral given in equation (16) may be written as,

$$\int_\Gamma \frac{X(t)\cos\theta}{t - z}dt = -\frac{i}{a}[S_1 + (z^2 + R^2(1 - 2\cos 2\alpha))S_2 + (z^4 + R^2(z^2 + R^2)(1 - 2\cos 2\alpha))S_3 - (z^2 - b^2)(z^2 + R^2)S_4]. \quad (17)$$

Constants C_0, C_2 and D_0 given in equation (16) are obtained using the above boundary conditions,

$$D_0 = \frac{\sigma_{ye}}{a\pi}(H_1 + H_2S_4) - C_0, \quad (18)$$

$$C_2 = \frac{R^2\sigma_{ye}}{a\pi}(H_3 + H_4S_4) - C_0R^2\cos 2\alpha = \frac{R^2\sigma_{ye}}{ia\pi}C_{33}, \quad (19)$$

$$C_0 = \frac{\sigma_{ye}}{a\pi(3 - \cos 2\alpha)}\left(\frac{S_1}{R^2} + 4\sin^2\alpha S_2 + R^2(2 - 3\cos 2\alpha)S_3 + b^2\left(S_4 + \overline{S_4}\right) - 2R^2\cos^2\alpha\overline{S_4} + 2H_1 - H_3 - H_4S_4 + H_2\left(S_4 + \overline{S_4}\right)\right) = \frac{\sigma_{ye}}{ia\pi}C_{44}, \quad (20)$$

$$H_1 = S_2 + 2R^2\sin^2\alpha S_3, \quad (21)$$

$$H_2 = -2R^2\cos^2\alpha + b^2, \quad (22)$$

$$H_3 = \frac{S_1}{R^2} + 2\sin^2\alpha S_2 - \frac{R^2}{2}(2\cos 2\alpha - \sin^2 2\alpha)S_3, \quad (23)$$

$$H_4 = \frac{R^2}{2}\left(3\sin^2 2\alpha - 4\cos^2\alpha\left(1 - e^{-2i\alpha}\right)\right). \tag{24}$$

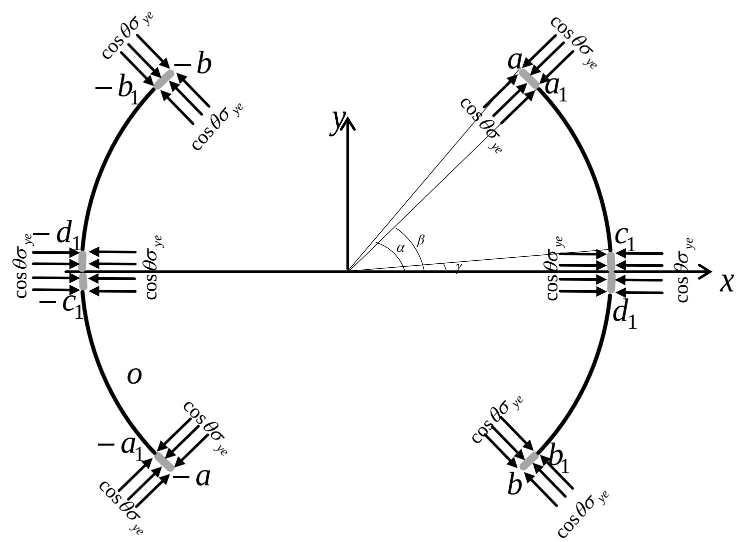

Fig. 6. Configuration of the closing case for $\cos\theta\sigma_{ye}$ loading

Thus, the final expression of the complex potential function for this case is then obtained by putting equations (17 – 24) in equation (16),

$$\Phi_{B_2}(z) = -\frac{\sigma_{ye}}{2a\pi X(z)}[S_1 + (z^2 + R^2(1 - 2\cos 2\alpha))S_2 + (z^4 + R^2(z^2 + R^2)(1 - 2\cos 2\alpha))S_3 - (z^4 + z^2R^2 - b^2(z^2 + R^2))S_4] + \frac{C_0 z^2 + C_2}{2X(z)} + \frac{D_0}{2}. \tag{25}$$

The state of stress in the crack tip $a = Re^{i\alpha}$ for the present case may be obtained on inserting the value of $\Phi_B(z)$ from equation (25) in equation (41) as,

$$K^I_{B_2} = \frac{\sigma_{ye}\sqrt{R}}{aie^{i\alpha}\sqrt{2\pi\sin 2\alpha}}\left[\frac{S_1}{R^2} + (1 - e^{-2i\alpha})S_2 - R^2e^{-2i\alpha}S_3 - R^2\left(e^{4i\alpha} - 1 + 2i\sin 2\alpha\right)S_4 - C_{44}e^{2i\alpha} - C_{33}\right]. \tag{26}$$

4. Numerical Study

A numerical study is carried out in this section to study the efficiency and accuracy of the analytical results obtained in the previous sections for various stress profiles. Analytical and numerical results for yield zone length have been acquired by superposing the solutions of two sub-problems, Subproblem-A (opening case) and Subproblem-B (closing case).

Case of $\sin\theta\sigma_{ye}$. The length of yield zones at the crack tip, $\boldsymbol{a}$, due to the stress distribution $\mathbf{\sin\theta\sigma_{ye}}$ is obtained by ensuring the Dugdale hypothesis that the stresses remain finite in the vicinity of the crack. Which is governed by the equation, $(\boldsymbol{K^m_A})_{\boldsymbol{I}} = \boldsymbol{K^I_{B_1}}$ and $(\boldsymbol{K^n_A})_{\boldsymbol{I}} = \boldsymbol{K^I_{B_1}}$. Thus, using equations (2), (4) and (15) one can obtain two non-linear equations corresponding to two different stress profiles discussed in section 3.1 as,

$$\left(1-2H^2+e^{2i\alpha}\right)\left(\frac{\sigma_\infty}{\sigma_{ye}}\right)_m$$
$$=-\frac{2-H^2}{\alpha\pi}\left[\frac{S_1}{R^2}-\left(1+e^{-2i\alpha}\right)S_2+R^2S_3e^{-2i\alpha}-R^2\left(e^{4i\alpha}-1-2i\sin2\alpha\right)S_4-C_{00}e^{2i\alpha}-C_{22}\right], \tag{27}$$

$$\left(\left(1+e^{2i\alpha}-2H^2\right)\left(\frac{2+\cos2\xi\cos2\alpha}{2-H^2}-i\frac{\sin2\xi\cos2\alpha}{H^2}\right)-\frac{2e^{2i\xi}}{e^{2i\alpha}}\right)\left(\frac{\sigma_\infty}{\sigma_{ye}}\right)_n$$
$$=-\frac{4(2-H^2)}{\alpha\pi}\left[\frac{S_1}{R^2}-(1+e^{-2i\alpha})S_2+R^2e^{-2i\alpha}S_3-R^2(e^{4i\alpha}-1-2i\sin2\alpha)S_4-C_{00}e^{2i\alpha}-C_{22}\right]. \tag{28}$$

It is almost impossible to solve the non-linear equations (27) and (28) in terms of yield zone length. However, normalized yield zone length at each crack tip is evaluated numerically against the applied load ratio $\frac{\sigma_\infty}{\sigma_{ye}}$ for each stress profile and reported graphically.

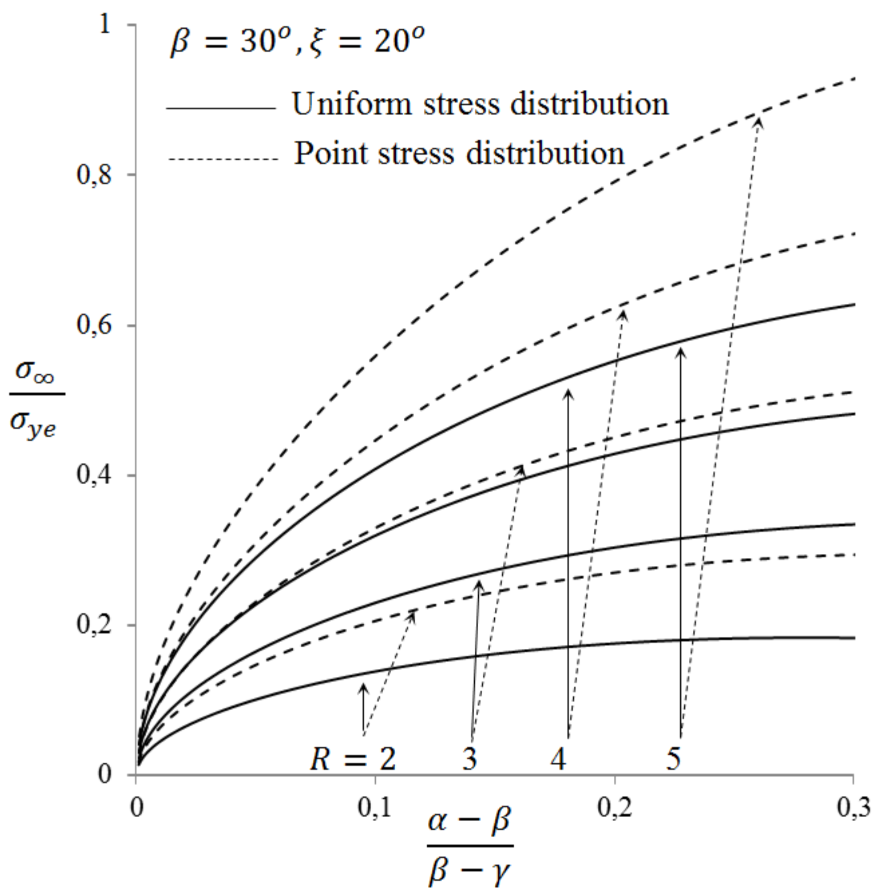

Fig. 7. $\frac{\sigma_\infty}{\sigma_{ye}}$ versus $\frac{\alpha-\beta}{\beta-\gamma}$ for the case of $\sin\theta\sigma_{ye}$ at different crack radius

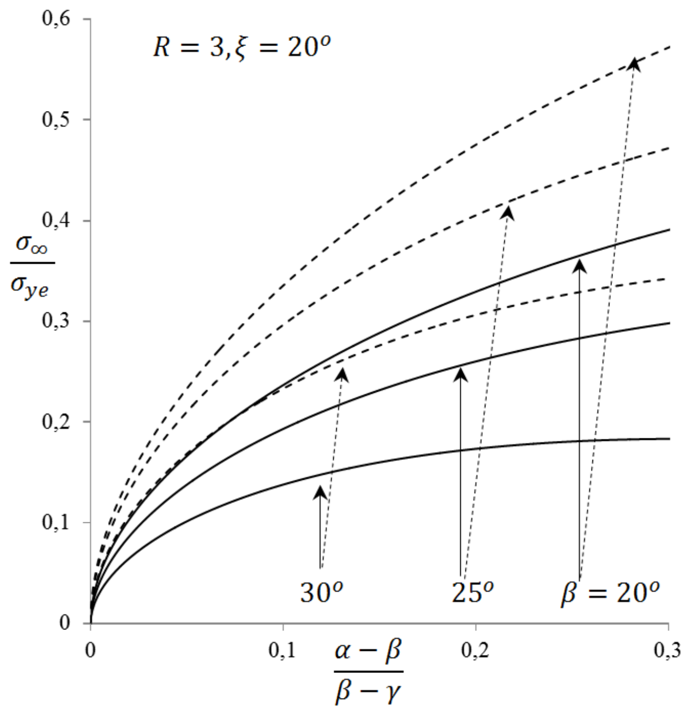

Fig. 8. $\frac{\sigma_\infty}{\sigma_{ye}}$ versus $\frac{\alpha-\beta}{\beta-\gamma}$ for the case of $\sin\theta\sigma_{ye}$ at different crack length

Figure 7 shows the behavior of normalized yield zone length, $\frac{R(\alpha-\beta)}{R(\beta-\gamma)}$, with respect to change in applied load ratio on the increasing radius of the circle (on which cracks lie). Increasing radius means an increase in inter crack distance. In the case of $R = 2$ (angle γ is very small) plate shows a low bearing capacity vis a vis $R = 5$ (γ is much larger) and much more significant in case of stress distribution act at an angle ξ. Further, it may be noted that the load applied at the boundary of the plate is significantly different in both the stress profiles. Hence, the plate under stress distribution act at an angle ξ be considered in a much safer position in the presence of the cracks as compared to the case of uniform stress distribution.

The same variation has been plotted in Fig. 8. for different crack length $R(\beta - \gamma)$, means increasing crack length. It has been observed that as the crack length increases, the load-bearing capacity of the plate decreases, which means that bigger cracks are more dangerous for the safe operation of the structures. In other words, the figure shows that the length of the plastically deformed region is more at each tip of bigger cracks as compared to the smaller ones for the fixed load required ratio $\left(\frac{\sigma_\infty}{\sigma_{ye}} = 0.1, say\right)$.

The effect of increasing angle of point stress applied at the boundary of the plate, in the case of four circular-arc cracks, is given in Fig. 9. It is found that as the angle ξ of stress distribution is increased, the residual strength of the plate also increases.

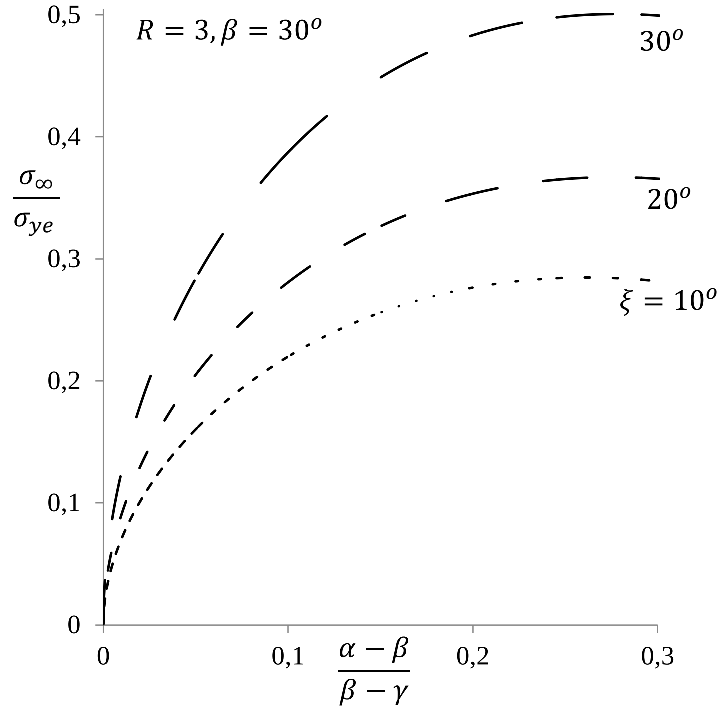

Fig. 9. $\frac{\sigma_\infty}{\sigma_{ye}}$ versus $\frac{\alpha-\beta}{\beta-\gamma}$ for $\sin\theta\sigma_{ye}$ at different angles ξ

Case of $\cos\theta\sigma_{ye}$. The length of developed yield enclaves for the case when yield stress distribution acting on the yield zones is varying as $\mathbf{cos\theta\sigma_{ye}}$ obtained in this section using the Dugdale hypothesis. Therefore, using equations (2), (4), and (26), one can get two non-linear equations corresponding to two different types of remote stress profiles in terms of applied and yield stress. These equations are

$$\left(1-2H^2+e^{2i\alpha}\right)\left(\frac{\sigma_\infty}{\sigma_{ye}}\right)_m = -\frac{2-H^2}{i\alpha\pi}\left[\frac{S_1}{R^2}+\left(1-e^{-2i\alpha}\right)S_2-R^2e^{-2i\alpha}S_3-R^2\left(e^{4i\alpha}-1+2i\sin2\alpha\right)S_4-C_{44}e^{2i\alpha}-C_{33}\right], \tag{29}$$

$$\left(1+e^{2i\alpha}-2H^2\right)\left(\frac{2+\cos2\xi\cos2\alpha}{2-H^2}-i\frac{\sin2\xi\cos2\alpha}{H^2})-\frac{2e^{2i\xi}}{e^{2i\alpha}}\right)\left(\frac{\sigma_\infty}{\sigma_{ye}}\right)_n = -\frac{4(2-H^2)}{i\alpha\pi}\left[\frac{S_1}{R^2}+(1-e^{-2i\alpha})S_2-R^2e^{-2i\alpha}S_3-R^2(e^{4i\alpha}-1+2i\sin2\alpha)S_4-C_{44}e^{2i\alpha}-C_{33}\right]. \tag{30}$$

Yield zone length developed at the crack tip, a, may be calculated from equations (29) and (30) corresponding to two different stress profiles of remotely applied stresses. Yield zone length at crack tip a is normalized with the corresponding crack length. In the following figures, normalised yield zone lengths are presented graphically with respect to the increasing values of the applied load ratio.

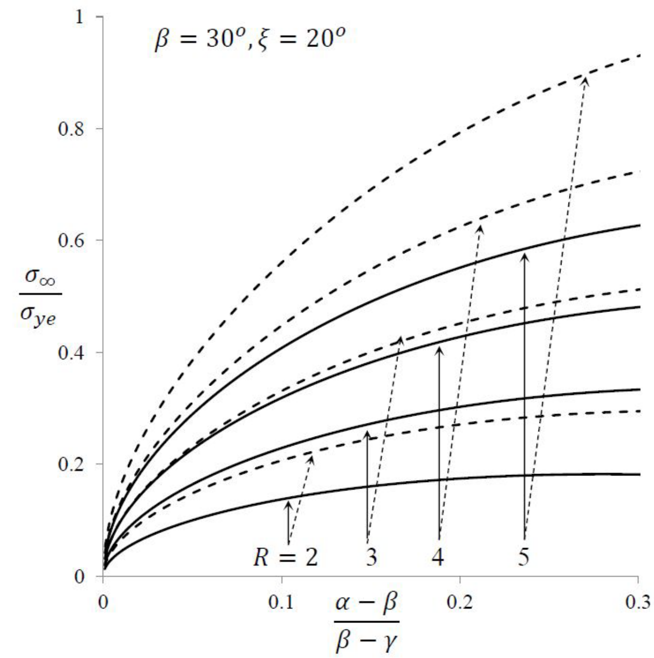

Fig. 10. $\frac{\sigma_\infty}{\sigma_{ye}}$ versus $\frac{\alpha-\beta}{\beta-\gamma}$ for stress profile $\cos\theta\, \sigma_{ye}$

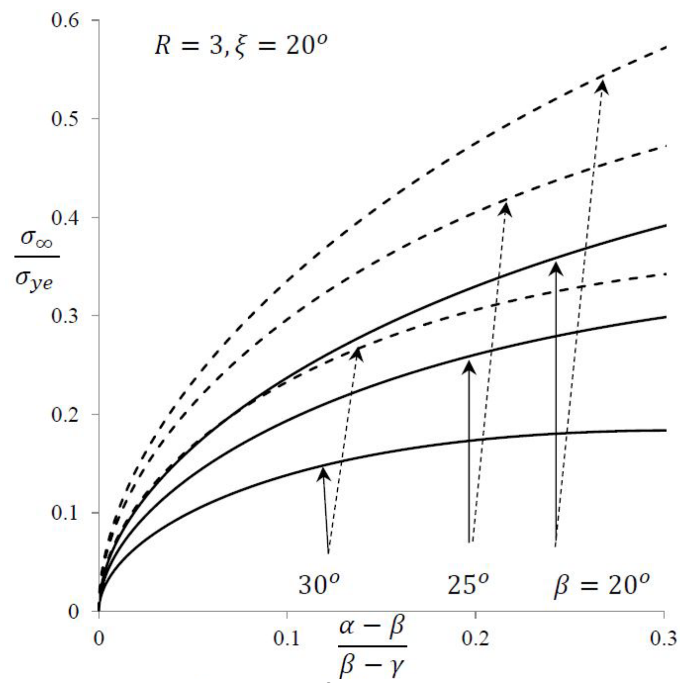

Fig. 11. $\frac{\sigma_\infty}{\sigma_{ye}}$ versus $\frac{\alpha-\beta}{\beta-\gamma}$ for stress profile $\cos\theta\, \sigma_{ye}$

Figure 10 shows the variation of sizes of normalized yield zone length with increasing values of applied stresses at crack tip $a = Re^{i\alpha}$ for different crack radius. Solid lines show the case of uniform stress distribution, while dashed lines show the evidence of stress distribution act at an angle ξ. It has been observed from the figure that the length of the yield zone increases as the stress applied at the infinite boundary of the plate is increased. Therefore, the load-carrying capacity of the plate is more in case of stress distribution act at an angle ξ in comparison to the case of uniform remote stress distribution.

Figure 11 shows the variation between applied load ratio with normalized yield zone length for increasing crack angles β. The load-carrying capacity of the plate becomes larger in case of the small cracks ($\beta = 20°$) as compared to the big cracks ($\beta = 30°$). Moreover, the less load-bearing capacity of the plate is seen in the case of uniform stress distribution in comparison to the case of stress distribution act at an angle ξ.

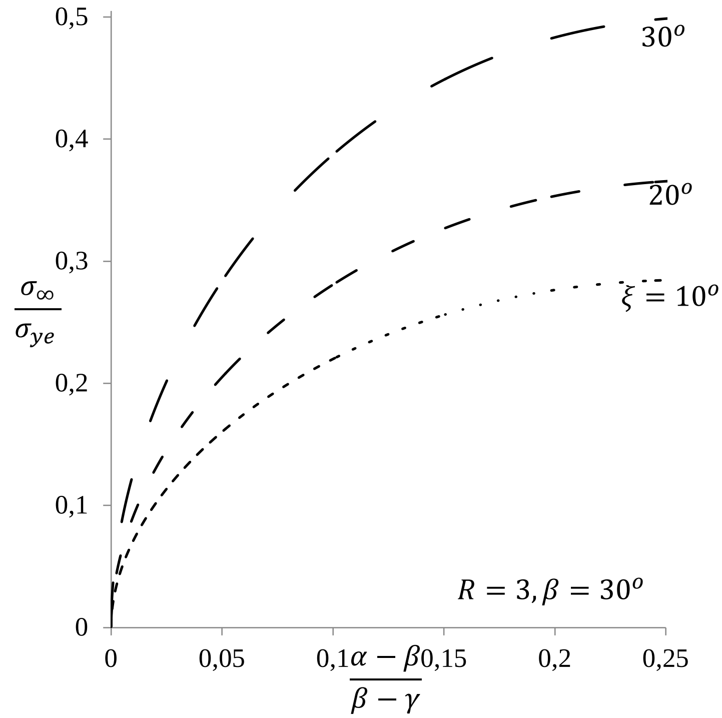

Fig. 12. $\frac{\sigma_\infty}{\sigma_{ye}}$ versus $\frac{\alpha-\beta}{\beta-\gamma}$ for different angles ξ

Finally, variation has been plotted in Fig. 12 between yield zone length and applied load ratio at different angles ξ. It is observed that as the angle ξ increases the load-bearing capacity of the plate will increases.

5. Conclusions

We considered the problem of multiple circular arc-cracks with coalesced yield zones. Analytical expressions for complex potential functions and stress intensity factors, for multiple circular-arc crack problems, were obtained for different types of mechanical loading conditions at the infinite boundary of the plate and variable yield stress distribution on the rims of yield zones. The analytical expressions for the opening-mode stress intensity factors given in equations (2), (4) are validated with the results provided by Tada [24]. The numerical study is carried out in the previous section to investigate the behaviour of yield zone length under variable loading conditions. It is seen that the yield zone length in the case of uniform stress distribution is larger as compared to point stress distribution. It is observed that as the angle of point stress distribution increases yield zone length decreases.

Acknowledgement*. Authors are grateful to the referees and the editor for their suggestions, which improved the understandability of the paper.*

References

[1] Dugdale DS. Yielding of steel sheets containing slits. *J. Mech. Phys. of Solids*. 1960;8(2): 100-104.
[2] Smith E. The extension of circular-arc cracks in anti-plane strain deformation. *Int. J. Engg. Sci.* 1969;7(9): 973-991.
[3] Chen YZ. New singular integral equations for circular arc crack and rigid line problem. *Eng. Frac. Mech.* 1994;47(1): 139-145.
[4] Chen YZ, Hasebe N. Fredholm integral equation for the multiple circular arc crack problem in plane elasticity. *Archieve of Applied Mechanics*. 1997;67: 433-446.
[5] Bhargava RR, Kumar R. Two equal symmetric circular arc cracks in an elastic medium - the Dugdale approach. *J. of Eng. Math*. 1998;34: 359-368.
[6] Bhargava RD, Narayan R. Circular inhomogeneity and two cocentric symmetric circular arc cracks problem in an infinite isotropic elastic plate under tension. *Int. J. Fract*. 1975;11: 509-520.
[7] Jagannadham K. Two cocentric circular arc cracks in anti-plane strain. *Eng. Fract. Mech*. 1977;9: 211-215.
[8] Zhang XS. The new general solutions of an infinite plate weakend by a circular-arc crack of mode I, II, and III. *Eng. Fract. Mech.* 1989;34(2): 275-282.
[9] Shish YC, Lin YJ. An infinitely large plate weakened by a circular-arc crack subjected to partially distributed loads. *J. of Engineering Mathematics*. 2004;49: 1-18.
[10] Zhong Z, Meguid SA. Analysis of a circular arc-crack in piezoelectric materials. *International Journal of Fracture.* 1997;84: 143-158.
[11] Gao CF, Kessler H, Balke H. Green's functions for anti-plane deformations of a circular arc-crack at the interface of piezoelectric materials. *Archive of Applied Mechanics.* 2003;73: 467-480.
[12] Shen D, Fan T. Semi inverse method for solving circular arc crack problems. *Eng. Fract. Mech*. 2004;71(12): 1705-1724.
[13] Cheung YK, Woos CW, Wang YH. Stress intensity factor for a circular-arc crack by Boundary collocation method. *Eng. Frac. Mech.* 1989;34(4): 841-849.
[14] Bhargava RR, Kumar R. Dugdale model solution for an infinite plate with a circular arc crack. *Eng. Fract. Mech.* 1993;46(2): 256-273.
[15] Gdoutos EE, Kattis MA, Argyokosta VK, Koutsougeras TJ, Papanelopoulou MC. Two circular arc-cracks in an infinite elastic plate. *Eng. Fract. Mech.* 19991;39(4): 671-681.
[16] Bhargava RR, Hasan S. Arrest of opening of two circular-arc cracks with coalesced plastic zones. *Mechanics of Composite Materials*. 2001;37: 201-206.
[17] Pourseifi M, Rahimi AS. Ductile failure analysis of epoxy resin plates containing multiple circular arc cracks by means of the equivalent material concept. *International Journal of Mechanical and Materials Engineering*. 2021;16(1): 1-13.
[18] Shim DJ, Tang S, Kim TJ, Huh NS. Stress intensity factors for circular arc cracks in plates. In: *Proceedings of ASME, Pressure Vessels and Piping Conference PVP*. 2018.
[19] Milne-Thomson LM. *Plane Elastic System*. Springer; 1960.
[20] Muskhelishvili NI. *Some basic problems of mathematical theory of elasticity*. Leiden: P. Noordhoff; 1963.
[21] Akhtar N, Hasan S. Four circular-arc cracks with coalesced yield zones in an infinite plate: A theoretical approach. *Strength, Fracture and Complexity*. 2018;11(4): 279-294.
[22] Gdoutos EE. *Fracture Mechanics: An Introduction*. Springer; 2005.

[23] Byrd PF, Friedman MD. *Handbook of elliptical integrals for engineers and scientist*, Springer; 1971.
[24] Tada H, Paris PC, Erwin GR. *The stress analysis of cracks handbook*. 3rd ed. NY: ASME Press; 2000.

Appendix. A. Mathematical formulation for circular arc cracks

This appendix is given to discuss the theory and methodology for solving the circular-arc crack problem as given by Muskhelishvili [20], Thomson [19] without any change. Here, the hypothetical thing is that n circular-arc cracks L_i $(i = 1,2,3,\ldots,n)$ are appeared in an infinite isotropic elastic-perfectly plastic plate along with one and the same circle $|z| = R$.

In the two-dimensional theory of elasticity for isotropic plates, stresses $(\sigma_{rr}, \sigma_{\theta\theta}, \sigma_{r\theta})$ are expressed in terms of two Muskhelishvili's complex potentials $\Phi(z), \Psi(z)$ as:

$$\sigma_{rr} + \sigma_{\theta\theta} = 2[\Phi(z) + \overline{\Phi(z)}], \tag{31}$$

$$\sigma_{rr} + i\sigma_{r\theta} = \Phi(z) + \overline{\Phi(z)} - \bar{z}\overline{\Phi'(z)} - \frac{\bar{z}}{z}\overline{\Psi(z)}. \tag{32}$$

Prime and bar over a function denote its first-order derivative and complex conjugate respectively.

For the solution of circular-arc crack problems, instead of potential function $\Psi(z)$ a new complex potential function $\Omega(z)$, related to $\Phi(z)$ and $\Psi(z)$, may be introduced as,

$$\Omega(z) = \overline{\Phi}\left(\frac{R^2}{z}\right) - \frac{R^2}{z}\overline{\Phi'}\left(\frac{R^2}{z}\right) - \frac{R^2}{z^2}\overline{\Psi}\left(\frac{R^2}{z}\right). \tag{33}$$

Equation (32) is then re-written using equation (33) as

$$\sigma_{rr} + i\sigma_{r\theta} = \Phi(z) + \Omega\left(\frac{R^2}{\bar{z}}\right) + \bar{z}\left(\frac{\bar{z}}{R^2} - \frac{1}{z}\right)\overline{\Psi(z)}. \tag{34}$$

Under the assumption

$$\lim_{r\to R}\left\{e^{-i\theta}\left(\frac{r}{R^2} - \frac{1}{r}\right)\Psi(z)\right\} = 0,$$

equation (34) may be converted into two subproblems of linear relationship, (since $z\bar{z} = r^2$)

$$\Phi^+(t) + \Omega^-(t) = \sigma_{rr}^+ + i\sigma_{r\theta}^+, \quad \Phi^-(t) + \Omega^+(t) = \sigma_{rr}^- + i\sigma_{r\theta}^-, \tag{35}$$

where $t = Re^{i\theta}$ be any point on $L = \bigcup_{i=1}^{n} L_i$, $\sigma_{rr}^{\pm} + i\sigma_{r\theta}^{\pm}$ represent stress components acting over the rims of the crack L and superscript (+) and (-) refers to the value of t from the inside $(r < R)$ and from outside $(r > R)$ of the circle on which cracks exist.

Adding and subtracting the equations in Eq.(35), one gets

$$[\Phi(t) + \Omega(t)]^+ = 2p(t), \quad [\Phi(t) + \Omega(t)]^- = 2q(t), \tag{36}$$

where

$$2p(t) = (\sigma_{rr}^+ + \sigma_{rr}^-) + i(\sigma_{r\theta}^+ + \sigma_{r\theta}^-), \quad 2q(t) = (\sigma_{rr}^+ - \sigma_{rr}^-) + i(\sigma_{r\theta}^+ - \sigma_{r\theta}^-). \tag{37}$$

In the absence of the body forces, the general solution of the boundary value problems expressed in Eq. (36) may be written directly from [20], as

$$\Phi(z) = \Phi_0(z) + \frac{1}{2X(z)}\left\{P_n(z) + \frac{D_1}{z} + \frac{D_2}{z^2}\right\} + \frac{D_0}{2} + \frac{\overline{\Gamma'}}{2z^2}, \tag{38}$$

$$\Omega(z)=\Omega_0(z)+\frac{1}{2X(z)}\left\{P_n(z)+\frac{D_1}{z}+\frac{D_2}{z^2}\right\}-\frac{D_0}{2}-\frac{\overline{\Gamma'}}{2z^2}, \tag{39}$$

where

$$\Phi_0(z)=\frac{1}{2\pi i X(z)}\int_L\frac{X(t)p(t)dt}{t-z}+\frac{1}{2\pi i}\int_L\frac{q(t)dt}{t-z},$$

$$\Omega_0(z)=\frac{1}{2\pi i X(z)}\int_L\frac{X(t)p(t)dt}{t-z}-\frac{1}{2\pi i}\int_L\frac{q(t)dt}{t-z},$$

$$X(z)=\prod_{k=1}^{n}\sqrt{z-a_k}\sqrt{z-b_k},$$

$$P_n(z)=C_0z^n+C_1z^{n-1}+C_2z^{n-2}+\cdots,$$

a_k, b_k denotes the endpoints of k^{th} crack.

Constants $D_i(i=0,1,2)$ and polynomial $P_n(z)$ are determined from the boundary conditions of the considered problem and the condition of single valuedness of displacement around the rims of the cracks or cuts,

$$2(\kappa+1)\int_{L_i}\frac{P_n(z)}{X(z)}dz+\kappa\int_{L_i}[\Phi_0^+(z)-\Phi_0^-(z)]dz+\int_{L_i}[\Omega_0^+(z)-\Omega_0^-(z)]dz=0. \tag{40}$$

Stress intensity factor for mode-I type deformation at each crack tip $z=a$ and $z=b$ may be calculated from the formulae given in [4],

$$K=K_1-iK_2=-2\sqrt{2\pi}\lim_{z\to a}\sqrt{(z-a)e^{-i\left(\frac{\pi}{2}+\alpha\right)}}\Phi(z), \tag{41}$$

$$K=K_1-iK_2=2\sqrt{2\pi}\lim_{z\to b}\sqrt{(z-b)e^{-i\left(\frac{3\pi}{2}-\alpha\right)}}\Phi(z). \tag{42}$$

Mathematical formulations given in this appendix are taken from [19], [20], and [4] to make the paper easily understandable and self-sufficient.

Appendix B. List of constants

$D_i(i=0,1,2), C_i(i=0,1,2)$	constants of the problem.
E	Young's modulus.
$F(\theta,k), E(\theta,k), \Pi(\theta,\alpha^2,k)$	incomplete elliptic integral of first, second and third kind, respectively.
$F(k), E(k)$	complete elliptic integral of first, second kind, respectively.
$L_i(i=1,2,3,4)$	circular-arc cracks.
$P_n(z)$	polynomial of degree *n*.
$p(t), q(t)$	applied stresses on the yield zones.
$z=re^{i\theta}$	complex variable.
Γ'	$-\frac{1}{2}(N_1-N_2)e^{-2i\alpha}, N_1$ and N_2 are the values of principal stresses at infinity, α be the angle between N_1 and the ox-axis.

$\Gamma_i (i = 1,2,\ldots,6)$	developed plastic/ yield zones.
$\Omega(z) = \omega'(z), \Phi(z) = \phi'(z)$	complex stress functions.
γ	Poisson's ratio.
μ	shear modulus.
κ	$= \frac{3-\gamma}{1+\gamma}$ for the plane-stress,
	$= 3 - 4\gamma$ for the plane-strain.
$\sigma_{rr}, \sigma_{\theta\theta}, \sigma_{r\theta}$	components of stress in polar coordinates.
σ_∞	remotely applied stress at infinite boundary of the plate.
σ_{ye}	yield stress of the plate.